Discover Medicine

Research

Abnormal skeletal muscle and myocardial vasoreactivity manifests prior to heart failure in a diabetic cardiomyopathy rat model

Sadi Loai[1,2] · **Hai-Ling Margaret Cheng**[1,2,3]

Received: 1 August 2024 / Accepted: 1 January 2025
Published online: 06 January 2025
© The Author(s) 2025 OPEN

Abstract

Background Microvascular dysfunction (MVD) is a recognized sign of disease in heart failure progression. Intact blood vessels exhibit abnormal vasoreactivity in early stage, subsequently deteriorating to rarefaction and reduced perfusion. In managing heart failure with preserved ejection fraction (HFpEF), earlier diagnosis is key to improving management. In this study, we applied a steady-state blood-pool magnetic resonance imaging (MRI) method to investigate if it can sensitively detect abnormal leg muscle vasoreactivity, a sign of MVD, posited to manifest before structural and functional cardiac changes emerge in a diabetes model of HFpEF.

Methods Male and female Sprague–Dawley rats were maintained on either a high-fat, high-sugar diet or a control diet for 6 months after the induction of diabetes ($n = 5$ per group). Beginning at month 1 or 2 post-diabetes and every 2 months thereafter, rats underwent steady-state blood-pool MRI to assess vasoreactivity in the heart or skeletal muscle, respectively. A T1-reducing blood-pool agent was administered and the T1 relaxation time dynamically measured as animals breathed in elevated CO_2 levels to modulate vessels.

Results In male rats, the normally unresponsive heart to 10% CO_2 revealed a pro-vasoconstriction response beginning at 5 months post-diabetes. Abnormal leg skeletal muscle vasoreactivity appeared even earlier, at 2 months: the usual vasodilatory response to 5% CO_2 was interrupted with periods of vasoconstriction in diseased rats. In female rats, differences were observed between healthy and diseased animals only in the first 2 months post-diabetes and not later. In the heart, vasodilation to 10% CO_2 seen in healthy females was abolished in diabetic females. In skeletal muscle, 5% CO_2 was suboptimal in inducing reproducible vasoreactivity, but young diabetic females responded by vasodilation only.

Conclusions Abnormal vasoreactivity presented earlier than overt functional changes in both heart and skeletal muscle in diabetic cardiomyopathy, and steady-state blood-pool MRI offered early diagnosis of microvascular dysfunction.

Keywords Vasoreactivity · Microvascular dysfunction · Blood-pool T1 imaging · Gadofosveset · Heart · Skeletal muscle · Hypercapnia · Diabetes

✉ Hai-Ling Margaret Cheng, hailing.cheng@utoronto.ca | [1]Institute of Biomedical Engineering, University of Toronto, Toronto, ON, Canada. [2]Translational Biology & Engineering Program, Ted Rogers Centre for Heart Research, 661 University Avenue, Room 1433, Toronto, ON M5G 1M1, Canada. [3]The Edward S. Rogers Sr. Department of Electrical and Computer Engineering, University of Toronto, Toronto, ON, Canada.

1 Introduction

Heart failure with preserved ejection fraction (HFpEF) is a medical conundrum: it accounts for over half of all heart failure cases and continues to rise in prevalence, with diagnosis typically occurring at late stage when effective therapies are limited [1]. Left ventricular wall thickening, an enlarged left atrium, and abnormal flow dynamics through chambers—all late phenotypes of this silent, slowly progressing disease—are readily uncovered on routine echocardiography [2]. Yet, early tissue changes associated with HFpEF, such as microvascular dysfunction (MVD), interstitial fibrosis, and myocardial stiffening, are much more difficult to diagnose. Only within the past decade have more advanced techniques emerged for early detection, such as quantitative stress perfusion for confirming microvascular disease and endothelial dysfunction, extracellular volume (ECV) mapping for fibrosis, or cardiac elastography for detecting increased myocardial stiffness [3–5]. However, even with these advances, this cardio-centric diagnostic approach ignores the possibility that yet earlier symptoms beyond the heart may arise. Considering that the drivers of HFpEF are believed to reside with the comorbidities (hypertension, diabetes, obesity, kidney disease) that present alongside HFpEF [6–10], it is sensible to adopt a holistic approach to diagnosing HFpEF at early stage.

Impaired vasoreactivity, or loss of normal blood flow regulation due to MVD, has been implicated as an early hallmark of inflammatory diseases such as HFpEF [9]. Clearly, it cannot be limited to the heart. Recent experimental studies have confirmed the presence of skeletal muscle MVD, in the form of vascular smooth muscle thickening, that underlie reduced baseline perfusion in animals with diabetes-related HFpEF [11, 12]. In fact, a significant reduction in perfusion manifested only in the leg muscle and not in the myocardium [11], and it coincided with the common early symptom of exercise intolerance seen in preclinical subjects and in patients. Despite these findings, diagnostic imaging studies involving the detection of MVD have been confined strictly to the heart [13]. There has been no recognition in the literature that detecting skeletal muscle MVD may be a potential avenue for earlier or easier HFpEF diagnosis. The few studies on skeletal muscle MVD employed techniques sensitive to large blood vessels, instead of the microcirculation, and limited to subjects with late HFpEF [14, 15]. Due to the lack of studies on early MVD presentation in the body, there is currently no information on when leg muscle MVD emerges relative to myocardial MVD.

In this study, we investigated the temporal manifestation of leg skeletal muscle MVD compared to myocardial MVD in an established rodent model of diabetes-related HFpEF. To achieve this goal, we employed a previously published steady-state blood-pool magnetic resonance imaging (MRI) technique for non-invasively assessing vasoreactivity in any tissue [16]. Briefly, the steady-state blood-pool method employs a long-circulating, intravascular T1 contrast agent to saturate the signal inside blood vessels, thus providing a means to measure time-varying changes in microvascular blood volume. Unlike other microvascular MRI methods, such as BOLD (sensitized to deoxyhemoglobin) or ASL (sensitized to flow velocity), the blood-pool method detects strictly blood volume changes associated with vasoreactivity. It also provides unlimited depth penetration unavailable with invasive gold standard modalities such as laser Doppler perfusion. For the blood-pool contrast agent, we will employ gadofosveset (tradename: Ablavar), which binds reversibly to serum albumin; compared to ferumoxytol adopted in recent blood-pool MRI studies [17, 18], gadofosveset affords at least an order of magnitude higher sensitivity of detection, making it possible to discriminate vasomodulation present in low-perfusion tissue such as resting muscle [19]. To our knowledge, this is the first study to demonstrate, using a clinically translatable blood-pool MRI platform, that leg skeletal muscle MVD provides an earlier indication than myocardial MVD with respect to HFpEF progression.

2 Materials and methods

2.1 Animal preparation

This study was approved by the University of Toronto's Animal Care Committee (protocol #20012191). All procedures were conducted in accordance with the Canadian Council on Animal Care. A non-obese type II diabetes model was adopted, one that leads to diabetic cardiomyopathy of the HFpEF phenotype in rats [11, 12]. Six- to seven-week-old male and female Sprague Dawley rats (Charles River, Quebec, Canada) were housed two per cage with a 12:12-h light–dark cycle and constant room temperature (23 ± 1 °C). Rats were divided into four groups: diabetic male rats ($n = 5$) and diabetic female rats ($n = 5$) on a high-fat/high-sucrose diet containing 20.14 wt% sucrose and 20.68 wt%

lard (D12451, Research Diets Inc., USA), and control male rats ($n = 5$) and female rats ($n = 5$) on a calorie-matched control diet (D12450K, Research Diets Inc.; New Brunswick, NJ, USA). All rats were fed ad libitum for the full duration of the study and had free access to water. Diabetes was induced in a fashion similar to our previous studies, along with a full cardiac and metabolic characterization of the phenotype in both sexes [11, 12]. In brief, 2 weeks after acclimatization, all rats were fasted overnight, and the diabetic cohorts were injected intraperitoneally (IP) with a low dose of streptozotocin (STZ, 30 mg/kg, Millipore Sigma, 572201; Burlington, MA, USA) dissolved in a 0.1 M citrate buffer, pH 4.5. The control group underwent the same procedure but were given a vehicle injection (citrate buffer). A total of three STZ injections were given, spaced 2 weeks apart, to induce a state of hyperglycemia. Following the diabetes induction period, the diabetic cohort was monitored for 1 month to confirm the presence of type II diabetes. To ensure diabetes was maintained throughout the study, non-fasting blood glucose measurements (glucometer, Accu-Chek Aviva, Roche Canada; Laval, QC, Canada) from a tail vein prick were collected monthly. All timepoints mentioned in this study refer to months post-induction of diabetes.

2.2 Gas challenge

Animals were anesthetized on 5% isoflurane in room air (2 L/min) and then intubated with a 14–18-gauge angio-catheter prior to being transferred to the MRI bed. Respiration was maintained at 80 breaths/min. Animals were placed in a supine position inside the rat body coil and were maintained at 37 °C throughout imaging. Isoflurane was maintained at 1.5–2% throughout the imaging session. Vital signs (heart rate, blood oxygen saturation, respiration rate) were monitored in real-time throughout the imaging session using a rodent oximeter (MouseOX Plus, STARR Life Sciences; Oakmont, PA, USA) placed on the hind paw. A 24-gauge tail vein angio-catheter was inserted and secured for contrast agent injection. During the gas regime, animals always began on 21% O_2 and 79% N_2, which is referred to as "normoxia" for brevity. The cardiac hypercapnic-normoxic gas regime was conducted as described in our earlier study [20]. Very briefly, 10% CO_2 mixed with 21% oxygen (O_2) and balanced with 69% N_2 in a GSM-3 gas mixer (CWE Inc.; Ardmore, PA, USA) was directed to an intubated rat. The skeletal muscle hypercapnic-normoxic gas regime involved administering a mixture of 5% CO_2, 21% O_2, and balanced with 74% N_2. These hypercapnic-normoxic gas mixtures are referred to as "hypercapnia" for brevity. These gas levels (i.e. 10% CO_2 for the heart and 5% CO_2 for skeletal muscle) were determined through repeated tests to determine the lowest concentration of CO_2 needed to invoke a vasoactive response in that specific organ. Respiration was controlled via an MRI-compatible ventilator (MRI-1 Ventilator, CWE, Ardmore, PA, USA). Gadofosveset, a blood-pool T_1 contrast agent (Ablavar™, Lantheus; North Billerica, MA, USA), was injected intravenously as a bolus (0.3 mmol/kg) followed by a saline flush. A specialized cardiac gating software that utilizes respiratory motion only to retrospectively gate to the rodent`s heartbeat was used to reconstruct cardiac images in two phases of the cardiac cycle [21], peak-systole and end-diastole. In this study, all analysis was done on the end-diastolic phase of the cardiac cycle.

2.3 In-vivo cardiac MRI

Rats were positioned supine and head-first, with the heart centered inside the rat coil. A complete cardiac imaging protocol can be found in our previous study [20]. Briefly, imaging was performed on a 3 Tesla pre-clinical scanner (MR Solutions; Guildford, UK). Localizer scans were first acquired to determine placement of the imaging volume on the cardiothoracic region. The imaging-injection protocol consisted of: (1) baseline 3D T_1-weighted CINE in the true short-axis plane (FA = 15°, TR = 6 ms, TE = 2.79 ms, 1 average, field of view = 70 mm, 16 slices, slice thickness = 1 mm) and pre-injection T_1-mapping via a variable flip angle approach [22] (FA = 2°, 5°, 10°, 15°, 20°, TR = 7 ms, TE = 3.36 ms), (2) gadofosveset injection, and (3) 3D CINE repeated every 5 min. The gas challenge regime post-contrast consisted of 10 min at normocapnic-normoxia (21% O_2), followed by 10 min at 10% CO_2, and finally recovery normocapnic-normoxia for 10 min. To quantitatively measure vasoreactivity within the microvasculature, one requires a direct metric that correlates with only blood volume and is unaffected by other physiological variables. To address this need, Ganesh et al. proposed in 2017 a blood-pool MRI approach for measuring vasomodulation in the presence of changes in blood gases [16], first demonstrating in abdominal organs [16] and later in ischemic disease [23] and low-perfusion tissue (e.g. skeletal muscle) [19]. This approach utilized a blood-pool contrast agent (e.g. gadofosveset) to achieve stable signal in the blood pool and then measure changes in the T_1-weighted signal or T_1 relaxation time as the microvasculature reacts in response to an external stimulus. The goal is to quantify relative changes in microvascular blood volume post-stimulus to assess microvascular function. Imaging timepoints occurred at 1, 3, and 5 months post-diabetes. Male and female control groups at the 1 month timepoint were originally published in our previous study [20].

2.4 In-vivo skeletal muscle MRI

Rats were positioned supine and head-first, with the pelvis centered inside the rat coil. Localizer scans were first acquired to determine placement of the imaging volume on the skeletal muscle region. The imaging-injection protocol consisted of: (1) baseline 3D T_1-weighted spoiled gradient echo (FA = 20°, TR = 11 ms, TE = 5.25 ms, 3 averages, field of view = 100 mm, 16 slices, slice thickness = 1 mm) and pre-injection T_1-mapping via a variable flip angle approach [22] (FA = 2°, 3°, 10°, 20°, TR = 11 ms, TE = 5.25 ms), (2) gadofosveset injection, and (3) 3D T_1-weighted spoiled gradient echo repeated every 1 min 40 s. The gas challenge regime post-contrast consisted of 10 min at normocapnic-normoxia (21% O_2), followed by 10 min at 5% CO_2, and finally recovery normocapnic-normoxia for 10 min. Imaging timepoints occurred at 2, 4, and 6 months post-diabetes.

2.5 MRI data analysis

Quantitative data analysis was performed in-house using Matlab (v2022, MathWorks, Natick, MA, USA). Post-injection T_1 relaxation times were computed from pre-injection T_1 maps and post-injection signal intensity via the spoiled gradient echo signal equation [24]. Slice location for image analysis was consistent among all animals for cardiac and skeletal muscle imaging. Regions of interest (ROIs) were drawn manually around the septum, anterior, and posterior myocardial wall for cardiac imaging, and around the gracilis and gastrocnemius muscles for skeletal muscle imaging. T_1 relaxation times were averaged across all ROIs at individual time-points of the gas challenge protocol. Skeletal muscle analysis underwent an additional step that involved computing the partial derivative of T_1 with respect to time to assess vasomodulation. This partial derivative is essential to extracting vasomodulation in low perfusion tissue such as resting muscle [19].

2.6 Laser Doppler perfusion measurements

Changes observed on skeletal muscle MRI were validated with real-time perfusion measurements at endpoint using laser Doppler flowmetry (OxyFlo, Oxford Optronix; Abingdon, UK). A fiber-optic probe (250–450 µm diameter) was secured into the gastrocnemius muscle; perfusion in arbitrary units was measured dynamically as the rat underwent hypercapnic challenge. The OxyFlo system counts the number of red blood cells within a small volume around the probe tip and provides a measurement in blood perfusion units (BPU). The data was analyzed in LabChart Reader (ADInstruments, Sydney, Australia).

2.7 Statistical analysis

Differences in T_1 relaxation times before, during, and after the CO_2 challenge with respect to baseline values for each cohort of animals were analyzed using a repeated-measures analysis of variance (ANOVA) with post-hoc analysis based on the Fisher's Least Significant Difference test. Significance was reported at a p value of 5%.

3 Results

3.1 Cardiac muscle vasoreactivity

Representative cardiac T_1 maps from male and female cohorts at 1-month post-diabetes induction are shown in Fig. 1. Imaging timepoints were captured at baseline normocapnic-normoxia post-contrast (gadofosveset), after 5 min on 10% CO_2, after 10 min on 10% CO_2, and after 10 min on recovery normocapnic-normoxia. Consistent between sexes and across both control and diabetic groups was a clear reduction in septal blood volume (i.e. vasoconstriction) upon transitioning from hypercapnia to recovery normocapnic-normoxia, as measured through an increase in T_1 relaxation time. Only during hypercapnia did differences in reactivity emerge between groups. In the control cohorts, females exhibited a strong vasodilation response (T_1 decreased 19 ± 5%) after being exposed

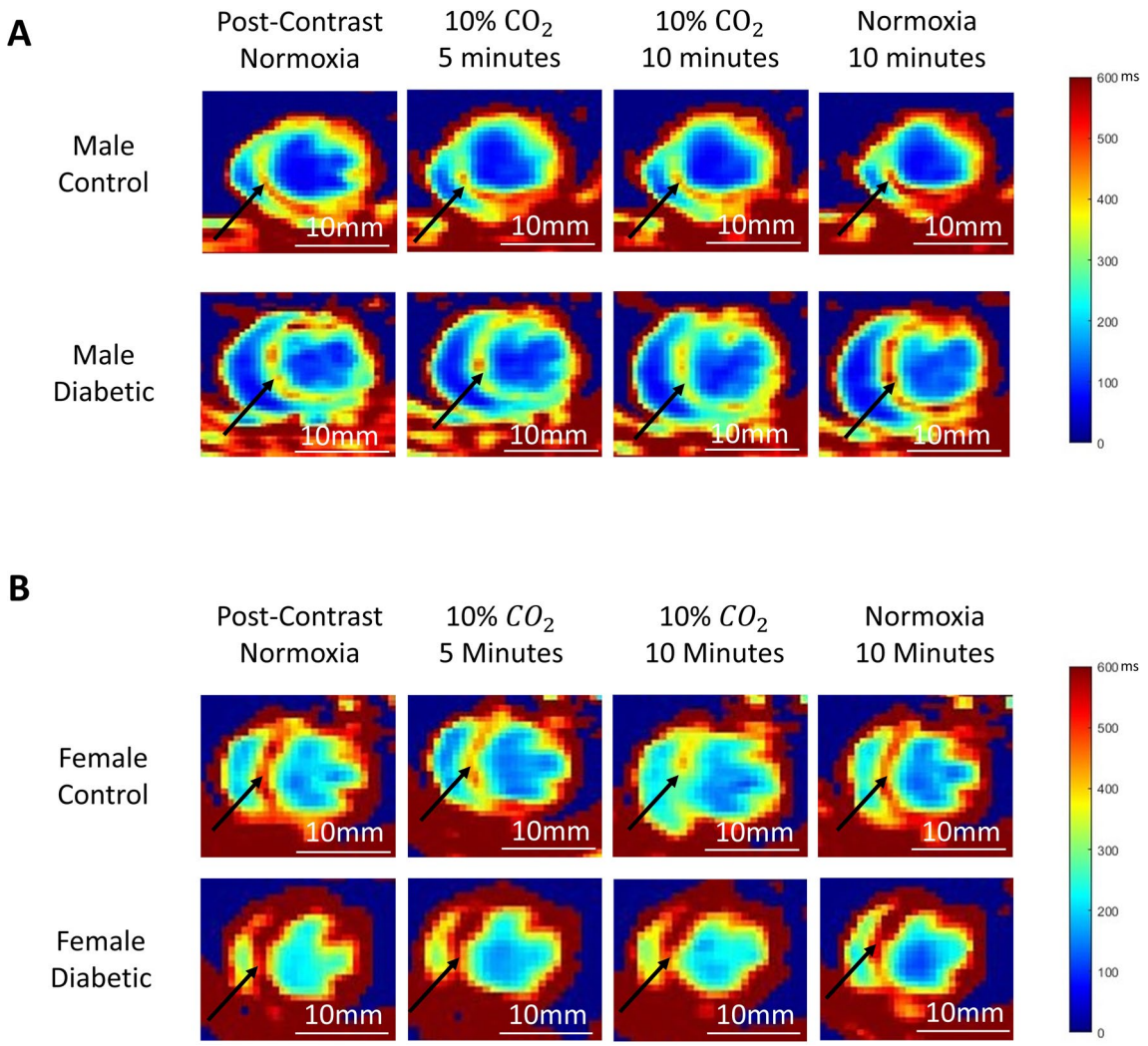

Fig. 1 Representative cardiac T_1 maps during different intervals of normoxia-hypercapnia-recovery normoxia gas stimuli in control and diabetic rats of both sexes. Young male (**A**) and female (**B**) control and diabetic rats at 1 month post-diabetes induction are shown. Black arrows highlight signal changes in the septum

to 10% CO_2 for 10 min, while males had minimal response to the hypercapnic challenge. In diabetic rats, both males and females exhibited insignificant vasodilation, with T_1 changes of $-9 \pm 5\%$ and $-8 \pm 3\%$, respectively.

Vasoreactivity also changed over time. Individual responses are shown in Fig. 2 for male rats and Fig. 3 for female rats, with mean percent changes in T_1 between successive gas challenges graphed in Fig. 4. In male control rats, who did not respond to hypercapnia at month 1, vasoreactivity continued to be minimal at months 3 and 5. On the other hand, in male diabetic rats, a clear and significant vasoconstriction to hypercapnia emerged at month 5 (T_1 increased $17 \pm 4\%$). For all male rats, vasoconstriction was always observed upon transitioning from hypercapnia to recovery normocapnic-normoxia. In female control rats, vasodilation in response to hypercapnia was seen at 1 month (T_1 decreased $19 \pm 5\%$), followed by increasingly dampened response at month 3 and 5. In contrast, female diabetic rats did not display vasodilation to hypercapnia at any timepoint. For all female rats, vasoconstriction always emerged on transition from hypercapnia to recovery normocapnic-normoxia.

Absolute T_1 relaxation times pre- and post-contrast injection along with percent change in T_1 across different gas intervals are shown in Tables 1 and 2 for male and female cohorts, respectively. A descriptive summary of these myocardial vasoreactivity trends is given in Table 3.

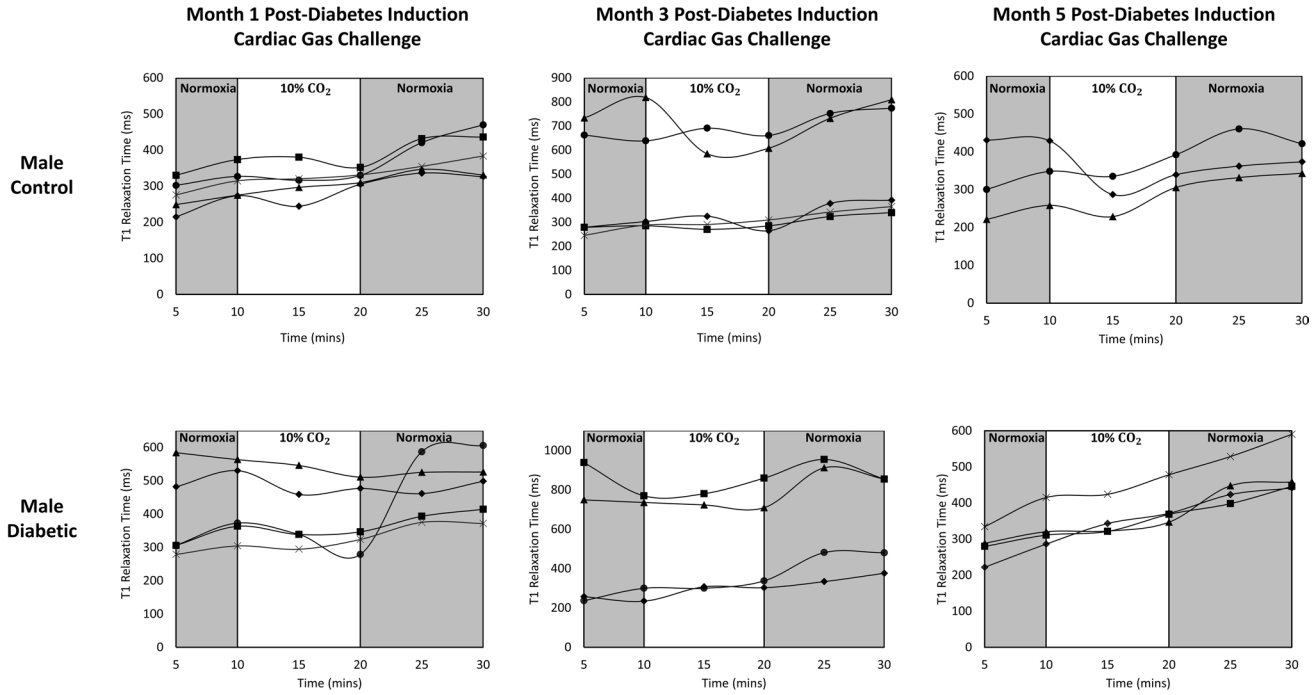

Fig. 2 T_1 measurements (ms) during different intervals of normoxia-hypercapnia-recovery normoxia gas stimuli in the myocardium of all male control and diabetic rats. T_1 measurements were averaged over the septum, anterior wall, and posterior wall for each animal at each time point [$n = 3$–5 male control (top) and $n = 4$–5 male diabetic (bottom)]

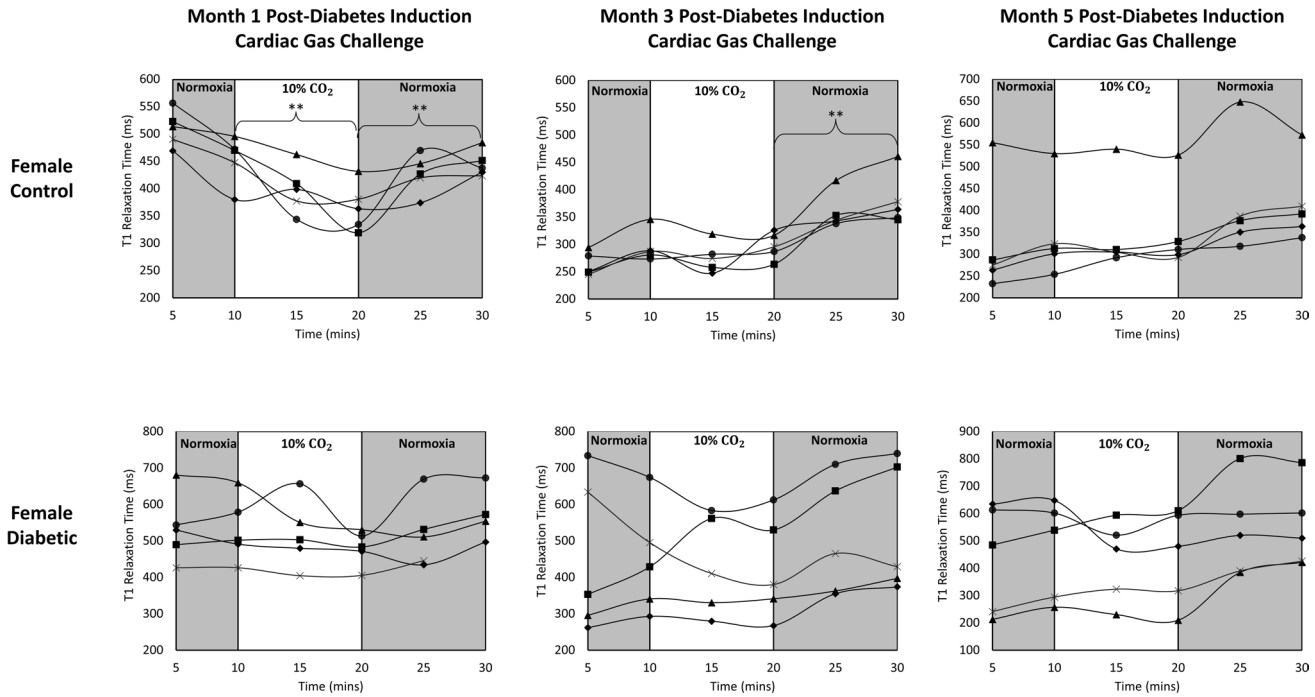

Fig. 3 T_1 measurements (ms) during different intervals of normoxia-hypercapnia-recovery normoxia gas stimuli in the myocardium of all female control and diabetic rats. T_1 measurements were averaged over the septum, anterior wall, and posterior wall for each animal at each time point [$n = 5$ female control (top) and $n = 5$ female diabetic (bottom)]. Significance is indicated relative to the start of each 10-min challenge (** $p < 0.01$)

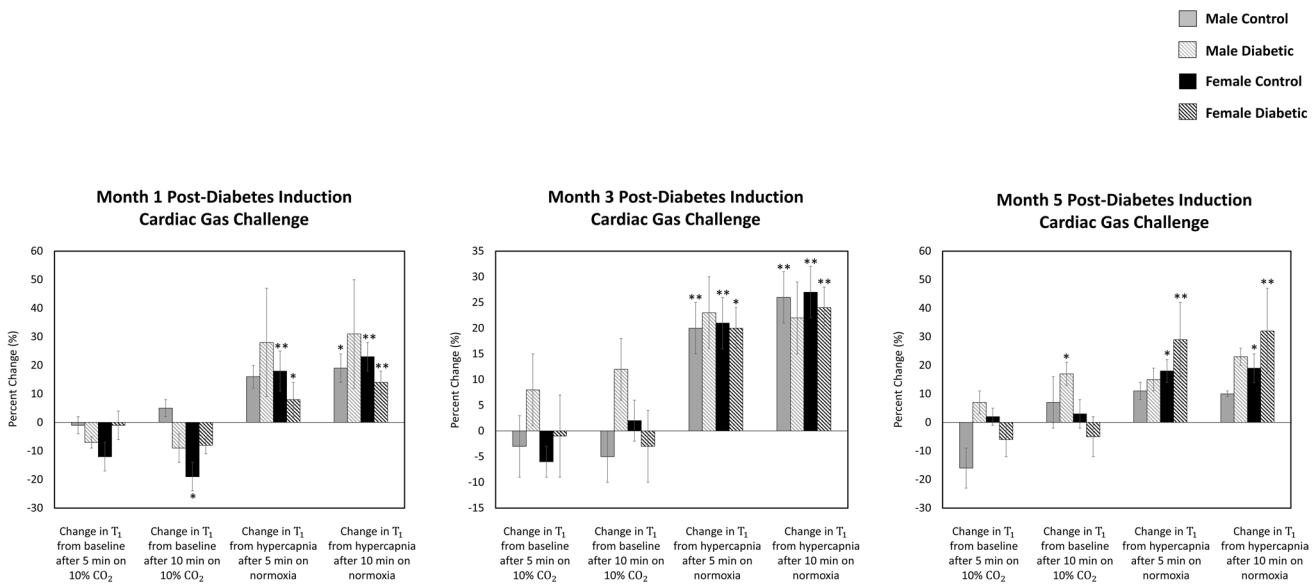

Fig. 4 Cardiac gas challenge and corresponding percent change (%) in T_1 relaxation time (ms) for all rats. Percent T_1 changes are calculated relative to the previous gas challenge, with significance indicated (* $p < 0.05$, ** $p < 0.01$). Data represented as mean ± SEM

Table 1 Myocardial T1 relaxation time evolution in response to gas challenge in male rats at different intervals post-diabetes

Male rats	Month 1		Month 3		Month 5	
Gas challenge sequence	Control ($n=5$)	Diabetic ($n=5$)	Control ($n=5$)	Diabetic ($n=4$)	Control ($n=3$)	Diabetic ($n=4$)
1. Pre-contrast T_1 (ms)	963 ± 55	1016 ± 24	1028 ± 49	1088 ± 37	1045 ± 14	1128 ± 65
2. Post-contrast T_1 (ms)—baseline	312 ± 16**	427 ± 45**	466 ± 99**	510 ± 121**	345 ± 40**	333 ± 25**
3. ΔT_1 from baseline after 5 min on 10% CO_2	−1 ± 3%	−7 ± 2%	−3 ± 6%	8 ± 7%	−16 ± 7%	7 ± 4%
4. ΔT_1 from baseline after 10 min on 10% CO_2	5 ± 3%	−9 ± 5%	−5 ± 5%	12 ± 6%	7 ± 9%	17 ± 4%*
5. ΔT_1 from 10% CO_2 after 5 min on normocapnic-normoxia	16 ± 4%	28 ± 19%	20 ± 5%**	23 ± 7%	11 ± 3%	15 ± 4%
6. ΔT_1 from 10% CO_2 after 10 min on normocapnic-normoxia	19 ± 5%*	31 ± 19%	26 ± 5%**	22 ± 7%	10 ± 1%	23 ± 3%

* $p < 0.05$, ** $p < 0.01$ relative to the previous gas challenge. Data represented as mean ± SEM

Table 2 Myocardial T1 relaxation time evolution in response to gas challenge in female rats at different intervals post-diabetes

Female rats	Month 1		Month 3		Month 5	
Gas challenge sequence	Control ($n=5$)	Diabetic ($n=5$)	Control ($n=5$)	Diabetic ($n=5$)	Control ($n=5$)	Diabetic ($n=5$)
1. Pre-contrast T_1 (ms)	1196 ± 29	1219 ± 50	1154 ± 19	1224 ± 56	990 ± 23	1265 ± 225
2. Post-contrast T_1 (ms)—baseline	453 ± 18**	531 ± 36**	295 ± 12**	474 ± 69**	344 ± 43**	468 ± 72**
3. ΔT_1 from baseline after 5 min on 10% CO_2	−12 ± 5%	−1 ± 5%	−6 ± 3%	−1 ± 8%	2 ± 3%	−6 ± 6%
4. ΔT_1 from baseline after 10 min on 10% CO_2	−19 ± 5%*	−8 ± 3%	2 ± 4%	−3 ± 7%	3 ± 5%	−5 ± 7%
5. ΔT_1 from 10% CO_2 after 5 min on normocapnic-normoxia	18 ± 7%**	8 ± 6%*	21 ± 5%**	20 ± 4%*	18 ± 4%*	29 ± 13%**
6. ΔT_1 from 10% CO_2 after 10 min on normocapnic-normoxia	23 ± 5%**	14 ± 4%**	27 ± 5%**	24 ± 4%**	19 ± 5%*	32 ± 15%**

* $p < 0.05$, ** $p < 0.01$ relative to the previous gas challenge. Data represented as mean ± SEM

Table 3 Summary of myocardial vasoreactivity in response to gas challenge

	Month 1 Post-diabetes	Month 3 Post-diabetes	Month 5 Post-diabetes
Male control	No change during hypercapnia Vasoconstriction in recovery normocapnic-normoxia (19 ± 5%)	No change during hypercapnia Vasoconstriction in recovery normocapnic-normoxia (26 ± 5%)	No change during hypercapnia Vasoconstriction in recovery normocapnic-normoxia (10 ± 1%)
Male diabetic	No change during hypercapnia Vasoconstriction in recovery normocapnic-normoxia (31 ± 19%)	No change during hypercapnia Vasoconstriction in recovery normocapnic-normoxia (22 ± 7%)	Vasoconstriction during hypercapnia (17% ± 4%) Vasoconstriction in recovery normocapnic-normoxia (23 ± 3%)
Female control	Vasodilation during hypercapnia (19 ± 5%) Vasoconstriction in recovery normocapnic-normoxia (23 ± 5%)	No change during hypercapnia Vasoconstriction in recovery normocapnic-normoxia (27 ± 5%)	No change during hypercapnia Vasoconstriction in recovery normocapnic-normoxia (19 ± 5%)
Female diabetic	No change during hypercapnia Vasoconstriction in recovery normocapnic-normoxia (14 ± 4%)	No change during hypercapnia Vasoconstriction in recovery normocapnic-normoxia (24 ± 4%)	No change during hypercapnia Vasoconstriction in recovery normocapnic-normoxia (32 ± 15%)

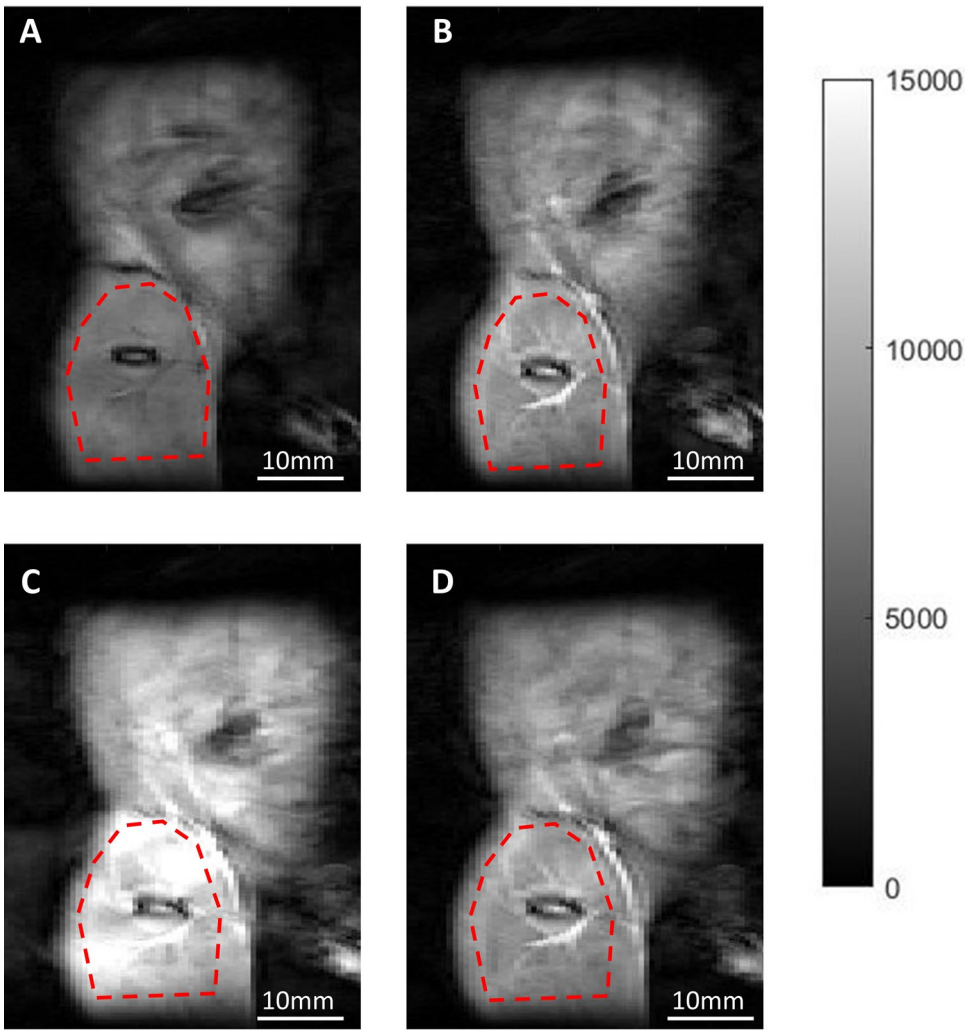

Fig. 5 Representative skeletal muscle T_1-weighted spoiled-gradient echo images during different intervals of normoxia-hypercapnia-recovery normoxia gas stimuli in a young male control rat. Images depict the leg muscle pre-contrast injection (**A**), post-contrast injection after 10 min on normocapnic-normoxia (**B**), after 10 min on 5% CO_2 (**C**), and after 6 min on recovery normocapnic-normoxia (**D**). Dotted red line represents the region of interest where measurements were collected

3.2 Skeletal muscle vasoreactivity

Representative leg skeletal muscle T_1-weighted images from a male control rat at the 2-month post-diabetes timepoint are shown in Fig. 5. Timepoints were captured at baseline normocapnic-normoxia pre-contrast (gadofosveset), baseline normocapnic-normoxia post-contrast, after 10 min on 5% CO_2, and after 6 min on recovery normocapnic-normoxia. A clear contrast increase was observed in the leg muscle, first from accumulation of blood-pool contrast agent and then from vasodilation on hypercapnia. The final transition from hypercapnia to recovery normocapnic-normoxia saw a reduction of contrast, indicating vasoconstriction.

Vasoreactivity also changed over time. MRI analysis for the partial derivative of T_1 with respect to time are shown in Figs. 6 and 7 for male and female rats, respectively. Color coding is used in these figures to facilitate identification of minimal vasoreactivity, dilation, and constriction. In male control rats, regardless of age, hypercapnia induced either no change or vasodilation followed by vasoconstriction on recovery normocapnic-normoxia. All male diabetic rats at month 2 displayed vasodilation to hypercapnia, but vasoconstriction set in part way into the hypercapnic interval. At month 4, this vasoconstriction occupied more of the hypercapnic interval, and by month 6, vasoconstriction was sometimes seen immediate to hypercapnic exposure before reversion to vasodilation. Mostly notably, unlike control male rats, diabetic male rats did not exhibit a consistent vasoconstriction response on recovery normocapnic-normoxia.

Female rats displayed more variable trends compared to males. In female rats, regardless of diabetes status or age, hypercapnia induced vasoconstriction, vasodilation, or a mixture of both. Furthermore, whereas control male rats

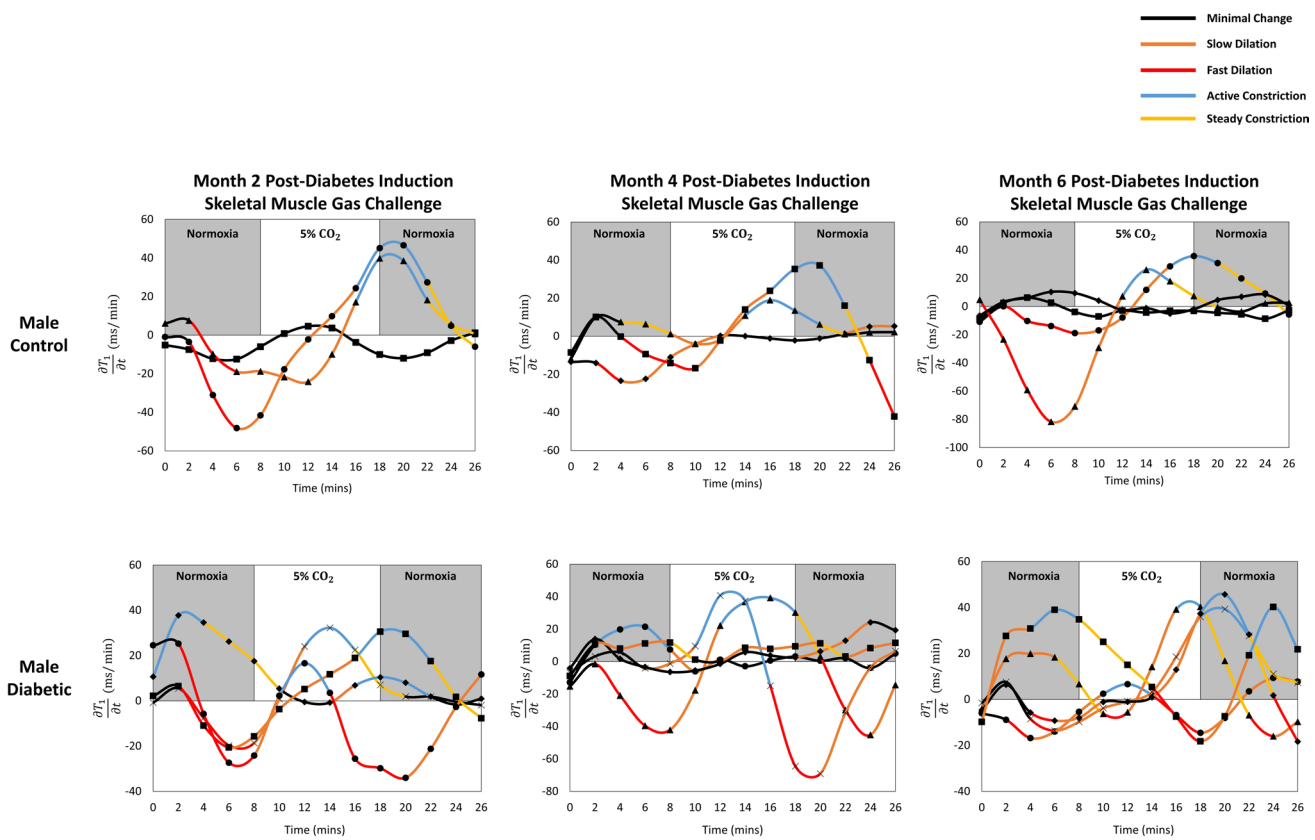

Fig. 6 MRI analysis in skeletal leg muscle for the partial derivative of T_1 with respect to time in male control ($n = 3–4$) and diabetic ($n = 4–5$) rats during different intervals of normoxia-hypercapnia-recovery normoxia gas stimuli for all timepoints. Color coded segments correspond to different microvascular vasoreactive responses

responded consistently to recovery normocapnic-normoxia by vasoconstricting, female control rats responded sometimes by vasoconstricting but more often by vasodilating. Strangely, some control females displayed no response at all throughout the study. Therefore, while diabetic males could be differentiated from control males by their variable response on recovery normocapnic-normoxia, diabetic females cannot be thus distinguished, since control females had inconsistent behavior. The single consistent observation in the female cohort was seen in young female diabetic rats at month 2: here, only vasodilation was observed throughout hypercapnia and recovery normocapnic-normoxia, with no sign of vasoconstriction.

A qualitative summary of skeletal muscle vasoreactivity in response to gas challenge is given in Table 4.

3.3 Laser Doppler perfusion validation

Representative laser Doppler measurements in skeletal muscle during different intervals of gas stimuli are displayed alongside the respective blood-pool response on MRI (Fig. 8). Despite that laser Doppler and MRI data were acquired in separate experimental sessions, the two modalities produced accordant assessment of vasoreactivity. The representative data displayed for a control male and a diabetic male rat at the 6-month timepoint shows an increase in laser Doppler-measured perfusion during periods of fast and slow dilation indicated on MRI, and a decrease in laser Doppler-measured perfusion during active and steady constriction indicated on MRI.

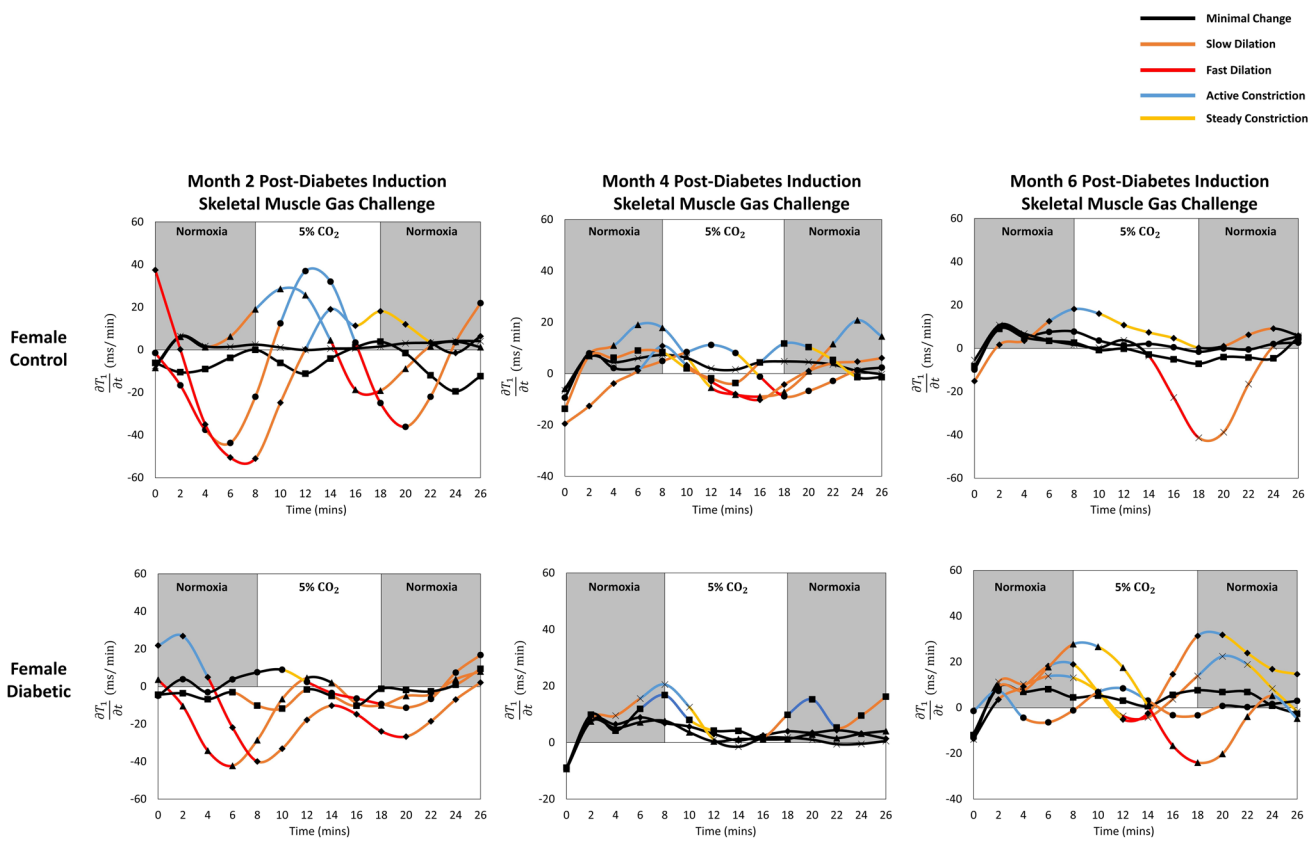

Fig. 7 MRI analysis in skeletal leg muscle for the partial derivative of T_1 with respect to time in female control ($n = 4–5$) and diabetic ($n = 4–5$) rats during different intervals of normoxia-hypercapnia-recovery normoxia gas stimuli for all timepoints. Color coded segments correspond to different microvascular vasoreactive response

4 Discussion

The increasing application of cardiac MRI stress testing for clinical assessment of MVD is premised on the suspected early presentation of myocardial MVD in the progression of HFpEF. Remarkably, no imaging study to date has characterized the role of skeletal muscle MVD in the early progression of HFpEF, nor has there been a comparison between skeletal muscle versus myocardial MVD. In this study, we provide the first demonstration that both skeletal muscle and myocardial microvascular vasoreactivity is altered in a non-obese rodent model of type II diabetes, prior to the development of heart failure symptoms.

In male rats, the normally unresponsive heart revealed a pro-vasoconstriction response to 10% CO_2 beginning at 5 months post-diabetes induction, whereas in leg skeletal muscle, the usual vasodilatory response to 5% CO_2 was interrupted with periods of vasoconstriction in diseased rats as early as 2 months post-diabetes. In female rats, a consistent difference between healthy and diseased animals was not obtained at later timepoints. However, within the first 2 months post-diabetes, the myocardial vasodilation seen in healthy animals was abolished in diabetic rats, and in skeletal muscle, the inconsistent vasoconstriction/dilation response to hypercapnia seen in healthy animals was replaced by vasodilation only in disease.

Cardiac assessment of microvascular reactivity across sex and time revealed several notable findings. Male and female control cohorts had different trends in their vasoactive response to hypercapnia. The hearts of male control rats did not respond to hypercapnia at all. A possible explanation is that male hearts have a larger microvascular reserve and do not need to vasodilate significantly in response to a stressor [25, 26]. Likewise, the hearts of female control rats did not respond to hypercapnia, except young females at the 1-month timepoint, who exhibited strong vasodilation to 10% CO_2. This response was expected and recently demonstrated in a clinical study [26], where healthy females with a median age of 35 years exhibited a strong vasodilation response when exposed to adenosine,

Table 4 Summary of skeletal muscle vasoreactivity in response to gas challenge

	Month 2 Post-diabetes	Month 4 Post-diabetes	Month 6 Post-diabetes
Male control	Vasodilation during hypercapnia Vasoconstriction in recovery normocapnic-normoxia	Vasodilation during hypercapnia Vasoconstriction in recovery normocapnic-normoxia	Vasodilation shortened during hypercapnia Vasoconstriction in recovery normocapnic-normoxia
Male diabetic	Inconsistent vasoconstriction/dilation during hypercapnia Inconsistent vasoconstriction/dilation during recovery normocapnic-normoxia	Inconsistent vasoconstriction/dilation during hypercapnia Inconsistent vasoconstriction/dilation during recovery normocapnic-normoxia	Inconsistent vasoconstriction/dilation during hypercapnia Inconsistent vasoconstriction/dilation during recovery normocapnic-normoxia
Female control	Inconsistent vasoconstriction/dilation during hypercapnia Inconsistent vasoconstriction/dilation in recovery normocapnic-normoxia	Inconsistent vasoconstriction/dilation during hypercapnia Inconsistent vasoconstriction/dilation in recovery normocapnic-normoxia	Inconsistent vasoconstriction/dilation during hypercapnia Inconsistent vasodilation in recovery normocapnic-normoxia
Female diabetic	Vasodilation during hypercapnia Vasodilation in recovery normocapnic-normoxia	Inconsistent vasoconstriction during hypercapnia Inconsistent vasoconstriction/dilation in recovery normocapnic-normoxia	Inconsistent vasoconstriction/dilation during hypercapnia Inconsistent vasoconstriction/dilation in recovery normocapnic-normoxia

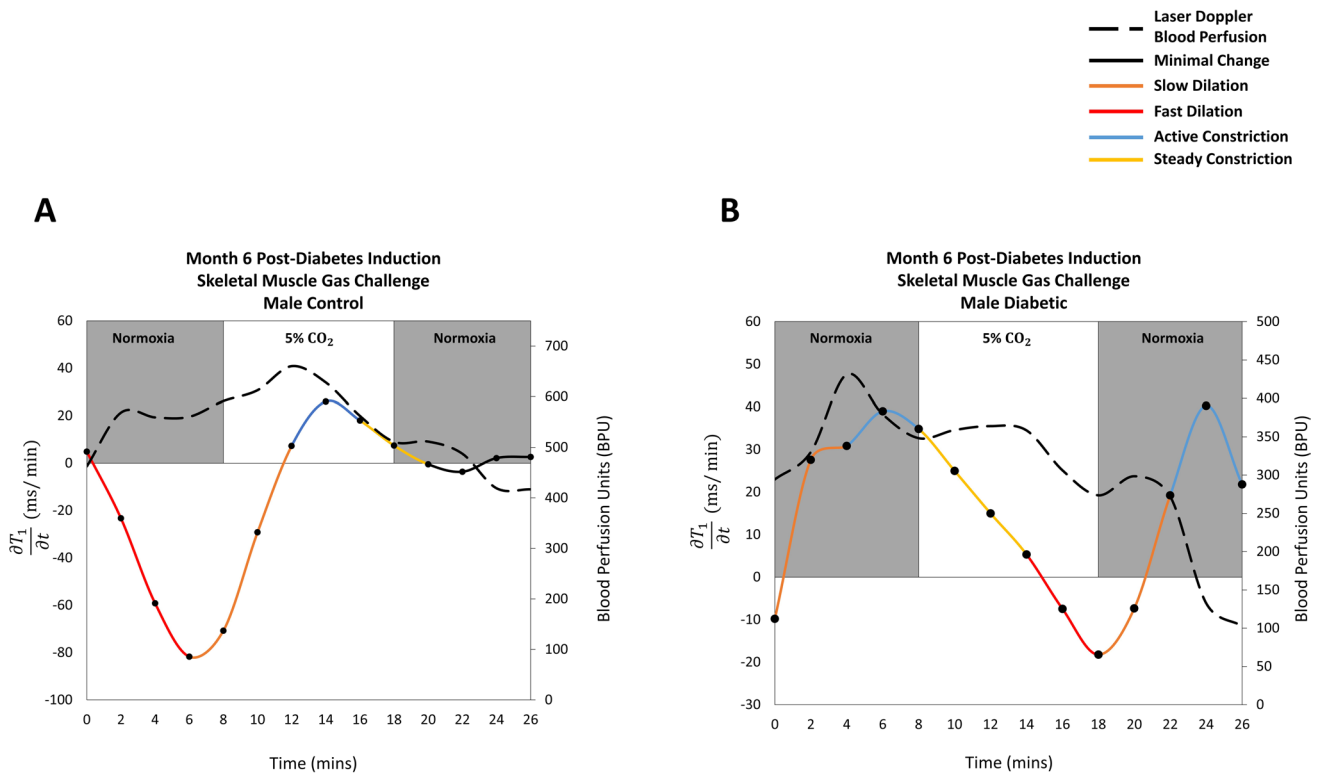

Fig. 8 Laser Doppler perfusion measurements compared to MRI measures of partial derivative of T_1 during different intervals of normoxia-hypercapnia-recovery normoxia gas stimuli in leg skeletal muscle of a representative male control (**A**) and a male diabetic rat (**B**). Measurements were collected at 6-month post-diabetes induction for each animal at a frequency of 10 Hz. Doppler perfusion is represented by black dashed lines with units in relative blood perfusion units (BPU)

compared to their male counterparts; this response was negatively correlated with increasing age. In diabetic rats, a difference between healthy and diseased hearts emerged in males at month 5, when significant vasoconstriction to hypercapnia appeared, indicating impairment to the microvascular bed. Female diabetics did not present a differential myocardial response compared to controls, as all diseased animals in this group did not respond to hypercapnia. Therefore, unlike male rats, where control animals had consistent trends and diabetic animals did not, female diabetic rats had consistent trends but female controls did not. This indicates that a hypercapnic threshold different from 10% CO_2 is required to distinguish disease in females as they age.

Skeletal muscle assessment of microvascular reactivity also revealed several notable findings. Control male rats consistently exhibited vasodilation to 5% CO_2 followed by vasoconstriction on recovery normocapnic-normoxia, but female controls demonstrated inconsistent response, with a mix of vasoconstriction and vasodilation throughout hypercapnia and recovery normocapnic-normoxia. This discrepancy may arise, again, from sex-based differential sensitivity thresholds to CO_2 due to hormonal factors or the structural composition of skeletal muscle fibers [27]. In diabetic animals, males lost their consistent vasodilatory response to hypercapnia at month 2. In diabetic females, it was difficult to judge when abnormal vasoreactivity set in, since a consistent response was not established in control females. However, it is noteworthy that female diabetic rats at month 2 vasodilated in response to 5% CO_2, without any vasoconstriction, not even on return to room air. Furthermore, the first presentation of MVD in skeletal muscle preceded any signs of exercise intolerance and histopathological damage. This finding further supports the claim that MVD in skeletal muscle is a precursor to exercise intolerance and heart failure in diabetic subjects.

Aside from the pathophysiological findings, it is worthwhile to examine more deeply the blood-pool MRI technique employed to assess vasoreactivity. As a blood-pool method, it is vastly different from common methods such as blood-oxygen-level-dependent (BOLD) MRI, which is influenced by blood oxygen saturation, blood flow velocity, hematocrit, and tissue oxygen consumption [28], or first-pass stress perfusion imaging that requires multiple injections of contrast agent to obtain a "baseline" perfusion and a "stress" perfusion estimate [29, 30]. By saturating the blood-pool with a T1 contrast agent, as originally proposed by Ganesh et al. [16] for vasoreactivity studies, T1 effects are dominated by

the amount of contrast agent in the vasculature, effectively providing a measurement of blood volume modulation independent of flow velocity. Increasingly more literature reports now utilize this method to assess injury and disease in ischemic settings [18, 23]. However, it is important to recognize that alternative methods, such as BOLD, can detect a subnormal myocardial oxygen reserve in HFpEF [31] and may provide valuable complementary information. One final note is that not all blood-pool contrast agents are created equal. While gadofosveset, the agent used in this study, has reversible binding with albumin and thereby gains access a greater pool of water protons (i.e. higher sensitivity), the current iron-oxide substitute ferumoxytol remains strictly inside blood vessels and is unable to yield substantial contrast changes from vasomodulation.

Another notable feature of our experiments is the use of altered inspired gases, rather than drugs, to modulate vascular response. Whether through hypercapnia or breathing maneuvers, an increasing number of studies now exploit this non-pharmacological approach to assess cardiac disease [32–34]. Altered levels of CO_2 and O_2 provide the flexibility of assessing bi-directional vasoreactivity [28, 35, 36], which pharmacological means cannot. The rich set of information gleaned from probing both the ability to dilate and to constrict can potentially paint a more fulsome understanding of microvascular disease. As an example, in this study, evaluating MVD in the skeletal muscle of male rats can be based not only on the consistent vasodilation to hypercapnia but also on the consistent vasoconstriction on recovery normocapnic-normoxia, both of which are abolished in diabetic males.

4.1 Limitations

The imaging procedures in this study were tailored to the heart and skeletal muscle. Because it was not possible to image both tissues in one session without exposing animals to excessive isoflurane, we alternated imaging the heart and muscle every month over 6 months, resulting in three imaging timepoints for each tissue. A second limitation is a small sample size ($n = 5$ per group). Although our MRI results were consistent with laser Doppler validation measurements, which met the technical objective of this study, using this new technique to explore differences in microvascular response between healthy and diseased tissue, and between male and female animals, uncovered large inter-subject variations. To establish statistical differences based on sex or disease status will require much larger sample sizes in future studies. Despite the low statistical power of the current study, it is important to appreciate that the proposed technology has equipped us to assess and discover unknown deep tissue microvascular dynamics on an individual level.

Another important future aim is to optimize the hypercapnic level for females, as 10% and 5% CO_2 elicited a reproducible myocardial and skeletal muscle response, respectively, in male rats only across all timepoints. It is noteworthy that throughout our initial protocol development, we observed that cardiac muscle was more resilient to the hypercapnia stress test and required a higher level of CO_2 to elicit a vasoactive response, compared to skeletal muscle. This form of stress testing had not been attempted before by any other group and clearly identified organ-specific CO_2 thresholds. In the future, we will need to assess all concentrations of CO_2 to determine sex-specific and organ-specific thresholds for the lowest possible CO_2 concentration that can evoke a vasodilatory response.

Lastly, non-gadolinium blood-pool agents [37] can potentially fill the gap left by gadofosveset, which was recently discontinued by the manufacturer and is no longer available for clinical use. In the meantime, clinical studies will necessitate the use of ferumoxytol (currently available for off-label use only in the USA), which is much less sensitive than gadofosveset, until a clinically approved reversible-albumin binding T1 agent similar to gadofosveset is again available. Preclinical studies can utilize a handful of blood-pool T1 agents available for animal studies. It is important to bear in mind that although the sensitivity of detection differs from one blood-pool agent to another, the technique presented in this study can be extended to any blood-pool agent.

5 Conclusion

This proof-of-concept study described a novel application of steady-state blood-pool stress MRI for the assessment and detection of impaired microvascular reactivity in cardiac and skeletal muscle in a rat model of type II diabetic heart failure. Results confirmed that our blood-pool stress MRI method could sensitively detect altered vasoreactivity in cardiac (high perfusion) and skeletal muscle (low perfusion) tissues. Results also suggested that abnormal vasoreactivity appeared in leg muscle before it appeared in the heart, and that both were precursors to cardiac structural and functional changes. This study underscores the importance of establishing reference baselines in terms of age and sex when performing

stress perfusion MRI. Our non-invasive MRI technology sets the foundation for a paradigm shift: impaired leg and cardiac muscle vasoreactivity can be detected during the early stages of HFpEF for early diagnosis and early intervention.

Author contributions SL contributed to the study design, performing all animal procedures and imaging, data analysis, statistical analysis, and drafting and editing of the manuscript. HLMC contributed to the overall direction, conceptualization, funding, study design, statistical analysis, and editing of the manuscript. All authors read and approved the final manuscript.

Funding This work was supported by the Canadian Institutes of Health Research [grant #PJT-175131 to H.L.M.C.]; Natural Sciences and Engineering Research Council of Canada [grant #RGPIN-2019-06137 to H.L.M.C.]; Canada Foundation for Innovation/Ontario Research Fund [grant #34038 to H.L.M.C.]; Dean's Spark Professorship [to H.L.M.C.]; Ted Rogers Centre for Heart Research PhD Education Fund [to S.L.].

Data availability The datasets used and/or analyzed during the current study are available from the corresponding author on reasonable request.

Declarations

Ethics approval and consent to participate This study was approved by the University of Toronto's Animal Care Committee (protocol #20012191). All procedures were conducted in accordance with the Canadian Council on Animal Care.

Competing interests The authors declare no competing interests.

Open Access This article is licensed under a Creative Commons Attribution-NonCommercial-NoDerivatives 4.0 International License, which permits any non-commercial use, sharing, distribution and reproduction in any medium or format, as long as you give appropriate credit to the original author(s) and the source, provide a link to the Creative Commons licence, and indicate if you modified the licensed material. You do not have permission under this licence to share adapted material derived from this article or parts of it. The images or other third party material in this article are included in the article's Creative Commons licence, unless indicated otherwise in a credit line to the material. If material is not included in the article's Creative Commons licence and your intended use is not permitted by statutory regulation or exceeds the permitted use, you will need to obtain permission directly from the copyright holder. To view a copy of this licence, visit http://creativecommons.org/licenses/by-nc-nd/4.0/.

References

1. Borlaug BA, Sharma K, Shah SJ, Ho JE. Heart failure with preserved ejection fraction: JACC scientific statement. J Am Coll Cardiol. 2023;81(18):1810–34.
2. van Ham WB, et al. Clinical phenotypes of heart failure with preserved ejection fraction to select preclinical animal models. JACC Basic Transl Sci. 2022;7(8):844–57.
3. Caenen A, et al. Ultrasound shear wave elastography in cardiology. JACC Cardiovasc Imaging. 2024;17(3):314–29.
4. Robinson AA, Chow K, Salerno M. Myocardial T1 and ECV measurement: underlying concepts and technical considerations. JACC Cardiovasc Imaging. 2019;12(11 Pt 2):2332–44.
5. van Dijk R, van Assen M, Vliegenthart R, de Bock GH, van der Harst P, Oudkerk M. Diagnostic performance of semi-quantitative and quantitative stress CMR perfusion analysis: a meta-analysis. J Cardiovasc Magn Reson. 2017;19(1):92.
6. Tourki B, Halade GV. Heart failure syndrome with preserved ejection fraction is a metabolic cluster of non-resolving inflammation in obesity. Front Cardiovasc Med. 2021;8: 695952.
7. Lin Y, Fu S, Yao Y, Li Y, Zhao Y, Luo L. Heart failure with preserved ejection fraction based on aging and comorbidities. J Transl Med. 2021;19(1):291.
8. La Gerche A, Howden EJ, Haykowsky MJ, Lewis GD, Levine BD, Kovacic JC. Heart failure with preserved ejection fraction as an exercise deficiency syndrome: JACC focus seminar 2/4. J Am Coll Cardiol. 2022;80(12):1177–91.
9. Bilak JM, Alam U, Miller CA, McCann GP, Arnold JR, Kanagala P. Microvascular dysfunction in heart failure with preserved ejection fraction: pathophysiology, assessment, prevalence and prognosis. Card Fail Rev. 2022;8: e24.
10. Abudureyimu M, et al. Heart failure with preserved ejection fraction (HFpEF) in type 2 diabetes mellitus: from pathophysiology to therapeutics. J Mol Cell Biol. 2022;14(5):28.
11. Loai S, Zhou Y-Q, Vollett KDW, Cheng H-LM. Skeletal muscle microvascular dysfunction manifests early in diabetic cardiomyopathy. Front Cardiovasc Med. 2021;8: 715400.
12. Loai S, et al. Microvascular dysfunction in skeletal muscle precedes myocardial vascular changes in diabetic cardiomyopathy: sex-dependent differences. Front Cardiovasc Med. 2022;9: 886687.
13. Vasiljevic Z, Krljanac G, Zdravkovic M, Lasica R, Trifunovic D, Asanin M. Coronary microcirculation in heart failure with preserved systolic function. Curr Pharm Des. 2018;24(25):2960–6.
14. Espino-Gonzalez E, et al. Abnormal skeletal muscle blood flow, contractile mechanics and fibre morphology in a rat model of obese-HFpEF. J Physiol. 2021;599(3):981–1001.
15. Francisco MA, et al. Locomotor muscle microvascular dysfunction in heart failure with preserved ejection fraction. Hypertens. 2021;78(6):1750–9.

16. Ganesh T, Estrada M, Yeger H, Duffin J, Cheng H-LM. A non-invasive magnetic resonance imaging approach for assessment of real-time microcirculation dynamics. Sci Rep. 2017;7(1):7468.
17. Colbert CM, et al. Ferumoxytol-enhanced magnetic resonance T1 reactivity for depiction of myocardial hypoperfusion. NMR Biomed. 2021;34(7): e4518.
18. Nguyen K-L, et al. Ferumoxytol-enhanced CMR for vasodilator stress testing: a feasibility study. JACC Cardiovasc Imaging. 2019;12:1582–4.
19. Zakher E, Ganesh T, Cheng HLM. A novel MRI analysis for assessment of microvascular vasomodulation in low-perfusion skeletal muscle. Sci Rep. 2020;10(1):4705.
20. Loai S, Qiang B, Laflamme MA, Cheng H-LM. Blood-pool MRI assessment of myocardial microvascular reactivity. Front Cardiovasc Med. 2023;10:1216587.
21. Daal MRR, et al. Quantification of mouse heart left ventricular function, myocardial strain, and hemodynamic forces by cardiovascular magnetic resonance imaging. J Vis Exp. 2021;171:2021.
22. Cheng H-LM, Wright GA. Rapid high-resolution T1 mapping by variable flip angles: accurate and precise measurements in the presence of radiofrequency field inhomogeneity. Magn Reson Med. 2006;55(3):566–74. https://doi.org/10.1002/mrm.20791.
23. Ganesh T, Zakher E, Estrada M, Cheng HLM. Assessment of microvascular dysfunction in acute limb ischemia-reperfusion injury. J Magn Reson Imaging. 2019;49(4):1174–85.
24. Tofts PS, et al. Estimating kinetic parameters from dynamic contrast-enhanced T1-weighted MRI of a diffusable tracer: standardized quantities and symbols. J Magn Reson Imaging. 1999;10(3):223–32.
25. Nickander J, Themudo R, Sigfridsson A, Xue H, Kellman P, Ugander M. Females have higher myocardial perfusion, blood volume and extracellular volume compared to males—an adenosine stress cardiovascular magnetic resonance study. Sci Rep. 2020;10(1):10380.
26. Brown LAE, et al. Sex- and age-specific normal values for automated quantitative pixel-wise myocardial perfusion cardiovascular magnetic resonance. Eur Heart J Cardiovasc Imaging. 2023;24(4):426–34.
27. Loai S. Blood-pool stress MRI as a tool for identifying early biomarkers of diabetic heart failure with preserved ejection fraction. PhD dissertation, University of Toronto, 2023.
28. Ganesh T, Estrada M, Duffin J, Cheng HL. T2* and T1 assessment of abdominal tissue response to graded hypoxia and hypercapnia using a controlled gas mixing circuit for small animals. J Magn Reson Imaging. 2016;44(2):305–16.
29. Lubbers DD, et al. The additional value of first pass myocardial perfusion imaging during peak dose of dobutamine stress cardiac MRI for the detection of myocardial ischemia. Int J Cardiovasc Imaging. 2008;24(1):69–76.
30. Cheng H-LM. Emerging MRI techniques for molecular and functional phenotyping of the diseased heart. Front Cardiovasc Med. 2022;9:1072828.
31. Fischer K, et al. Insights into myocardial oxygenation and cardiovascular magnetic resonance tissue biomarkers in heart failure with preserved ejection fraction. Circ Heart Fail. 2022;15(4): e008903.
32. Hillier E, et al. Heterogeneity of coronary vascular function and myocardial oxygenation in women with angina and non-obstructive coronary artery disease. Eur Heart J Cardiovasc Imaging. 2024;25(8):1136–43.
33. Hillier E, Covone J, Friedrich MG. Oxygenation-sensitive cardiac MRI with vasoactive breathing maneuvers for the non-invasive assessment of coronary microvascular dysfunction. J Vis Exp. 2022;186: e64149.
34. Kwiatkowski G, Kozerke S. Quantitative myocardial first-pass perfusion imaging of CO_2-induced vasodilation in rats. NMR Biomed. 2021;34(12): e4593.
35. Cheng H-LM. Effect of hyperoxia and hypercapnia on tissue oxygen and perfusion response in the normal liver and kidney. PLoS ONE. 2012;7(7): e40485.
36. Duffin J, Mikulis DJ, Fisher JA. Control of cerebral blood flow by blood gases. Front Physiol. 2021;12: 640075.
37. Vollett KDW, Cheng H-LM. Efficient one-step amide formation using amino porphyrins. Org Biomol Chem. 2024;22(31):6308–20.

Publisher's Note Springer Nature remains neutral with regard to jurisdictional claims in published maps and institutional affiliations.